國立交通大學

資訊科學與工程研究所

碩 士 論 文

手 持 裝 置 行 人 追 蹤 系 統

Pedestrian Tracking System for Handheld Devices –
Using Accelerometers and Magnetometers

研 究 生：陳依廷

指導教授：曾煜棋　教授

易志偉　教授

中 華 民 國　九 十 八 年 六 月

手持裝置行人追蹤系統
Pedestrian Tracking System for Handheld Devices – Using Accelerometers and Magnetometers

研 究 生：陳依廷　　Student：Yi-Ting Chen

指導教授：曾煜棋、易志偉　　Advisor：Yu-Chee Tseng、Chih-Wei Yi

國 立 交 通 大 學

資 訊 科 學 與 工 程 研 究 所

碩 士 論 文

A Thesis

Submitted to Institute of Computer Science and Engineering

College of Computer Science

National Chiao Tung University

in partial Fulfillment of the Requirements

for the Degree of

Master

in

Computer Science

June 2009

Hsinchu, Taiwan, Republic of China

中華民國九十八年六月

手持裝置行人追蹤系統

研究生：陳依廷　　指導教授：曾煜棋 教授

易志偉 教授

國立交通大學

資訊科學與工程研究所

摘要

為了改進全球定位系統的缺點，例如：定位準確度、室內訊號不良，近年來個人導航系統成為了一個熱門的研究題目。大部份的個人導航系統均以計步器為基礎並利用微機電系統實作，藉由在使用者身上黏貼微機電系統來收集、分析資料，來計算使用者行走的步數、距離及方向，以便追蹤使用者的移動路徑。微機電系統黏貼的位置可分為：腳或腳踝、腰間、手持…等，由於使用者的手會產生不規則的抖動或振動，因此實作手持裝置定位的難度，相較於其他黏貼位置來得更加困難。

在本研究中，利用微機電系統實作了手持裝置行人追蹤系統，所使用的裝置包括加速度計及磁力計；此系統包含了三個模組：計步模組、步距模組及方向模組。計步模組藉由檢查加速度資訊並抓取步行樣本，來偵測使用者是否有走路的行為，同時濾除使用者手部的振動對裝置造成的雜訊；步距模組利用計步模組所抓取的步行樣本來估算此樣本所對應的步距；方向模組則利用磁力強度和加速

度資訊來計算手持裝置的歐拉角和手持角度。

藉由整合上述三個模組的輸出資訊，我們實作了行人追蹤系統。使用者只需手持此系統的硬體裝置（約一般手持裝置大小），系統即可追蹤使用者的移動軌跡並輸出；此系統可應用在各種手持裝置上，進行室內及室外的個人定位；未來將會與全球定位系統整合，以改善全球定位系統之缺點，對於都市、室內及室外的個人導航都相當有幫助，同時也可應用於提供行動定位服務與家庭看護上。

關鍵字：個人導航系統、全球定位系統、加速度計、磁力計、計步器、微機電系統、室內/室外定位、行動定位服務

Pedestrian Tracking System for Handheld Devices – Using Accelerometers and Magnetometers

Student：Yi-Ting Chen　　Advisors：Prof. Yu-Chee Tseng

Prof. Chih-Wei Yi

Institutes of Computer Science and Engineering

National Chiao Tung University

Abstract

The Personal Navigation System (PNS) becomes a popular research topic recently because people want to improve the shortcomings of Global Positioning System (GPS) such as accuracy and indoor usability. A lot of such systems are pedometer-based system which could be implemented using Micro Electro-Mechanical Systems (MEMS) and attached to different positions on a human body. The handheld pedometer is less than other locations such as foot and waist because the device held by one's hand has more noises and it is more difficult to model the human walking pattern.

In this paper, a *Pedestrian Tracking System* (PTS) is designed for handheld devices and implemented using accelerometers and magnetometers. It is composed of three modules: stepping module, stride module and direction module. The stepping

module detects a step occurrence of user through pattern matching in acceleration and filters the noises like shaking and vibrations. The stride module acquires the parameters of a step pattern from stepping module, and calculate the corresponding stride length of the step pattern. The direction module uses magnetic intensity and accelerations to evaluate the Euler angles and holding angles of a device.

By integrating the outputs of stepping module, stride module and direction module, the Pedestrian Tracking System is implemented. This system, which can be embedded into cellphones or PDAs easily, is feasible for indoor or outdoor personal positioning with a given initial position. In the future, the PTS could be integrated with the GPS for improving the positioning accuracy of both. It is very helpful for personal navigation in urban areas, indoor and outdoor environments and could be applied in providing location based services and home healthcare, etc.

Keywords：Personal navigation system, global positioning system, accelerometer, magnetometer, pedometer, MEMS, indoor/outdoor location, location based services.

誌　　謝

非常感謝這兩年以來，曾煜棋教授以及易志偉教授的辛苦指導；兩位指導教授不僅在學業及研究上給予我許多的幫助與督導，同時在人生的方向也提供了良好的建議，並且提供了舒適的實驗室環境和充足的設備，讓我得以順利完成此篇論文。

此外，感謝實驗室的全體同學，兩年來給予我的幫助與鼓勵；藉由同學間互相勉勵、學習，促進彼此在各方面的進步，有了你們的陪伴，讓我的碩士生活變得更充實、更有意義。

最後，我要感謝我的家人以及所有關心我的朋友們，因為有你們的支持與關懷，才使我能夠不被困難打倒，並在挫折中學習、成長。謝謝大家，因為有你們的幫忙跟鼓勵，讓我在就讀碩士這兩年成長不少，變得更成熟、懂事，不僅學習到許多專業知識，也留下了許多美好的回憶。謝謝！

陳依廷 於

國立交通大學資訊科學與工程研究所碩士班

中華民國九十八年六月

Contents

List of Figures

List of Tables

Chapter 1

Introduction

By the evolution of semiconductor technology, the Micro Electro-Mechanical Systems (MEMS) are rising, too. The volume of MEMS becomes smaller and the capability becomes stronger. In addition, the accuracy is good enough for most applications. At the same time, the penetration of handheld devices such as PDAs and cellphones is above 100 percent and these handheld devices become one part of our daily life. Integrating inexpensive MEMS into handheld devices will not increase the weight, size and cost of the devices too much. Instead, these embedded MEMS can enhance the capability of handheld devices and provide users with more services.

The Global Positioning System (GPS) is so popular in recent years that new generation cellphones and PDAs have built-in GPS. Because weather or terrain will affect the quality of the satellite signal, commercial GPS, which has accuracy of about 10 meters, is not accurate enough for personal positioning. Besides, GPS does not work indoors because the signal is blocked by buildings. Therefore, hoping to overcome the shortcomings of GPS is getting considerable concern in the Personal Navigation System (PNS). A lot of PNS are pedometer-based systems which count how many steps a user takes for estimating his walking distance. Thus the pedometer is the key of the pedometer-based PNS because the accuracy of positioning depends on

the accuracy of step counters.

To track the trajectory of human, devices are attached to a human body. There are four wearing and holding positions where the devices attached to a human body: 1) instep or ankle [1], [2], [3]; 2) waist [4], [5]; 3) chest [6]; and 4) handheld, in the bottom-up order. The noises of the accelerometer will intensify with the raising of the attached position. While the accelerometer attached to the foot or ankle, there is a reset point in a human walking cycle when the foot fully touches the ground. The acceleration and velocity are zero at this moment. It helps the correction of the accumulative errors caused by the accelerometer. However, the chest and the waist cases do not have this characteristic to correct the accumulative errors. Little literature considers the handheld devices. This paper focuses on handheld devices, which have not only accumulative errors as the chest and the waist devices, but have additional vibrations caused by hands, it makes the outputs of device unstable and difficult to be processed.

In this paper, a tri-axial accelerometer and a tri-axial magnetometer are used for implementing an accurate *Pedestrian Tracking System* (PTS) for handheld devices. There are two advantages for positioning by handheld devices. First, the user does not need to attach devices to his body, so inconvenience will be reduced. Second, due to no need for wireless communication equipment in our system, the risk of disconnection or packet loss will be avoided. Furthermore, only a tri-axial accelerometer and a tri-axial magnetometer are used instead of relatively expensive gyroscopes in our system. Therefore, PTS is an economical handheld devices solution to track the trajectory of human.

This system is composed of three modules: step module, stride length module and direction module. They provide three essential information for pedestrian positioning: step count, stride length and walking direction, re-

spectively. By measuring the variation of accelerations during a human walking cycle, we find a human walking pattern. Based on this finding, assisting by noise filters, the step module can accurately detect steps. Most of the related works attached devices on waist, foot or chest. However, for handheld devices, detecting steps needs more effort because there are a lot of noises due to hand vibrations while the user is walking. It is easy to do a wrong judgement and the walking pattern is difficult to be recognized. This module checks the accelerometer outputs in real time and detects if there is a walking motion. It is capable to detect steps accurately in both flat walking and stair walking. Even the influence due to shaking devices and hand vibrations could be eliminated by the noise filters.

The second essential information for personal positioning is the distance, which means how long people (or automobile) moves from one location to another. Many different methods of estimating the displacement of the object are developed, such as acceleration double-integration, machine learning, Data Mining and the Regression Analysis. The integration method [2], [7], and the regression analysis [1], [5], [4] are common used in the relative researches. The former indicates the displacement of an object can be evaluated by double-integrating the acceleration data while it moves, it is useful for foot-mounted device because of the feature that the acceleration and velocity of foot are zero when subject static stands which is helpful for eliminating the accumulative errors in integration every step. But, the double-integration method is unsuitable for handheld posture.

To estimate the stride length (also called walking distance) of user, the Regression Analysis is used in this study. By observing the experimental statistics of step pattern, it is found that some parameters which are used for step detection and noise filtering are correlative with the stride length. After analyzing these parameters, the transform equation between the parameters

and stride length is derived, and the stride length could be estimated exactly through the transform equation. An experiment is performed to verify the accuracy of the stride length estimation equation in Section 5.3.

The last essential information for personal positioning is the walking direction which means the heading of people, and it affects the location determination of personal positioning. The magnetometer and gyroscope are common used in DR module for direction estimation, and serveral differences between these two MEMS are illustrated in Table 1.1.

Table 1.1: A comparison of magnetometer and gyroscope.

	Magnetometer	Gyroscope
Output	Magnetic field intensity	Angular velocity
Purpose	Calculate absolute direction	Calculate angle variation
Price	Low	High
Accuracy	Low	High
Disadvantage	Sensitive to magnetic force	Exist accumulative errors

Because the walking direction calculation module is developed for personal positioning, the absolute direction information is necessary. Thus, the magnetometer which provides absolute direction is elected to be the core of walking direction module.

The magnetometer which senses the magnetic field intensity of Earth is considered as the electronic compass. It has a maximum value while the axis points to North Pole of the Earth, it is called Earth vector. By calculating the rotation between Earth vector and measured magnetic vector, the orientation of device is estimated and represented in Euler angles: yaw, pitch and roll, and the yaw angle is considered as the walking direction. The relative changes of orientation between the user and the device also can be figured out by the relation among the components of accelerations.

For pedestrian, the step count, stride length, and the walking direction

information could be integrated into an Inertial Navigation System (INS) or Dead Reckoning (DR) module, which can provide relative moving information indoors or outdoors. Moreover, INS could be integrated with GPS to overcome the drawback of GPS. The integrated pedestrian navigation system is more suitable than any navigation system using GPS only. It has higher accuracy and shorter response time. An accurate positioning system plays an important role in location-based service systems, which are promising in the near future.

The rest of this paper is organized as follows. We introduce the relative researches briefly in Chapter 2. The system architecture and equipments of PTS are illustrated in Chapter 3. The methodology for detecting the walking cycle are described in Chapter 4. Chapter 5 describes how we estimate the stride length by using regression analysis. In Chapter 6, the methods of calculating walking direction, and the holding angle are introduced. The integrated system and the experimental results of it are illustrated in Chapter 7. Chapter 8 is our conclusions.

Chapter 2

Related Work

2.1 Step Detection

Step detection needs to judge whether a human is walking or not and calculate the steps by examining the data received from the MEMS attached to his body. There are three methods using these data to detect steps: peak detection, zero crossing detection and flat zone detection [4]. The zero crossing detection method has weak ability to filter noise because the user may shake the device unconsciously. The flat zone detection method is only suitable for foot-mounted case. Thus, the peak detection which detects the peaks of signal is used in this paper.

In [1], a tri-axial accelerometer and an uni-axial gyroscope are attached to a subject's foot instep. It defined a gait cycle as four phases and used a finite-state algorithm to detect the step occurrence. The angular velocity is used as the main information for step detection, hence the only axis of the gyroscope must be aligned to the subject's ankle rotation axis. By integrating the accelerometer and the gyroscope outputs, step detection becomes more accurate and the accumulative errors could be eliminated through the cooperation of these MEMS [2]. However, the gyroscope is more expensive than the accelerometer and there are accumulative errors when the user holds

the device in his hand.

From a waist-mounted accelerometer, [5] found that the variation of accelerations caused by walking is a sinusoid-like pattern occurring in both forward and vertical acceleration. To detect the positive and the negative peak pair in both axes, test the gradient from the positive to the negative peak in forward acceleration, then the step cycle is determined. [5] also used a gyroscope for estimating the gravity vector. The method used in waist-mounted devices can not be applied to handheld devices because the axes of waist-mounted devices are easy to be fixed by the belt clips, but the hand of human can not be fixed, causing unstable outputs of devices.

A human activity detection system was developed in [6]. The paper classified human behaviors such as walking, running and fall by testing the tri-axial accelerometer signals, the signal magnitude area and the signal magnitude vector, but it did not cope with the noises.

2.2 Stride Length Estimation

The stride duration, which indicate the duration from one step to the next, is considered as a factor of stride length estimation. Human spends little time from one step to another in high speed, that is, the faster human walks, the shorter the stride duration is. In [1], the stride duration was measured accurately by using a foot-mounted gyroscope, and the conversion equation between the stride length and durations obtained by using regression analysis. It needs to attached the gyroscope to user's insteps for measuring step duration. Because the stride length, which is equivalent to the displacement, is relative to the acceleration of subject, the accelerometer is used widely for evaluating the walking distance of human. Another parameters such as forward and vertical acceleration difference between the peak and trough in a step pattern are used in regression analysis [5]. The gyroscope and ac-

celerometer are used for calculating the vertical axis of subject and helping the horizontal axis calculation in this research. In [4], it used both the walking frequency, which is the reciprocal of the stride duration, and the variance of the accelerometer signals during one step as the elements of regression analysis.

By double-integrating the acceleration data while device moves, the displacement is obtained, and the flat-zone of acceleration which only appears in foot-mounted case is applied to correct the drifts in acceleration and velocity [2]. The acceleration of gravity also affect the result of acceleration integration. [7] used gyroscope and accelerometer to eliminate the gravity from the measured acceleration vector accurately by computing and tracking the orientation of device. It shows an excellent experimental results in horizontal plane moving, but it can't be applied in varied environments such as walking and driving.

2.3 Walking Direction Calculation

By double-integrating the acceleration acquired from a foot-mounted accelerometer, the foot sagittal orientation is calculated [1], and the 3-D displacements is also estimated [2]. But the method of integrating is unavailable in handheld posture as described in previous chapter. In [8], an uni-axial and a bi-axial magnetometer were attached to the chest of subject and measured the magnetic field for calculating the Euler angles. The rotation matrix between two magnetic field vectors which are measured at two moments is determined by the quaternion, and the Euler angles is obtained by the rotation matrix. However, it didn't consider the inclination and declination of Earth, which affect the measured magnetic field and change according to the longitude and latitude.

[6] used a chest-mounted tri-axial accelerometer to determine the human

falling direction, it is classified to only four directions: frontal, back, left and right. In [5], it first removes the gravitational acceleration, which is calculated by the waist-mounted accelerometer and gyroscope, from the measured acceleration, then used the principal component analysis to determine the forward direction of the subject. The forward direction in [5] indicates the angle difference between the heading of the device and the heading of the subject, it isn't the absolute walking direction. In [7], the accelerometer and gyroscope were used for tracking the orientation of the device, and it couldn't provide the absolute walking direction, too.

In [9], a digital compass was implemented by using a bi-axial accelerometer and a bi-axial magnetometer. The direction is represented in Euler angles, the pitch and roll angles are obtained by using the accelerometer outputs, and the yaw angle is calculated by pitch, roll and the bi-axial magnetometer outputs. Because there is only a bi-axial magnetometer, it couldn't cope with 3-D rotation. To deal with 3-D rotation, a tri-axial magnetometer and tri-axial accelerometer are used [10]. A smart toothbrush was developed to classify the brushing patterns by estimating the rotation of toothbrush. The method of calculating pitch and roll is same as [9], and the yaw angle is calculated by pitch, roll and the tri-axial magnetometer outputs.

Chapter 3

System Architecture

3.1 Instrumentation

An Inertial Measurement Unit (IMU), 3DM-GX1, MicroStrain Inc., is used in the PTS. It is composed of one tri-axial accelerometer, one tri-axial gyroscope and one tri-axial magnetometer, but only the accelerometer and magnetometer are utilized in our system. The x-axis of the accelerometer points forward of the device when it is placed on a flat plane, the y-axis points to the right of it, and the z-axis points downward, and the axes of the magnetometer align to those of accelerometer. The output range of the accelerometer is $\pm 5g$, the outputs of magnetometer is ± 1.2 Gauss, and the maximum sampling rate of both is 350Hz.

3.2 System Module

The architecture of our system is illustrated in Figure 3.1. A tri-axial accelerometer and a tri-axial magnetometer are used in the system. The Processing Unit (PU), such as notebooks and PDAs, read 3D accelerations and magnetic intensities from the accelerometer and magnetometer via RS-232 interface, then store them in a sample buffer. These signals are successively processed by three modules: the stepping module, stride module and direc-

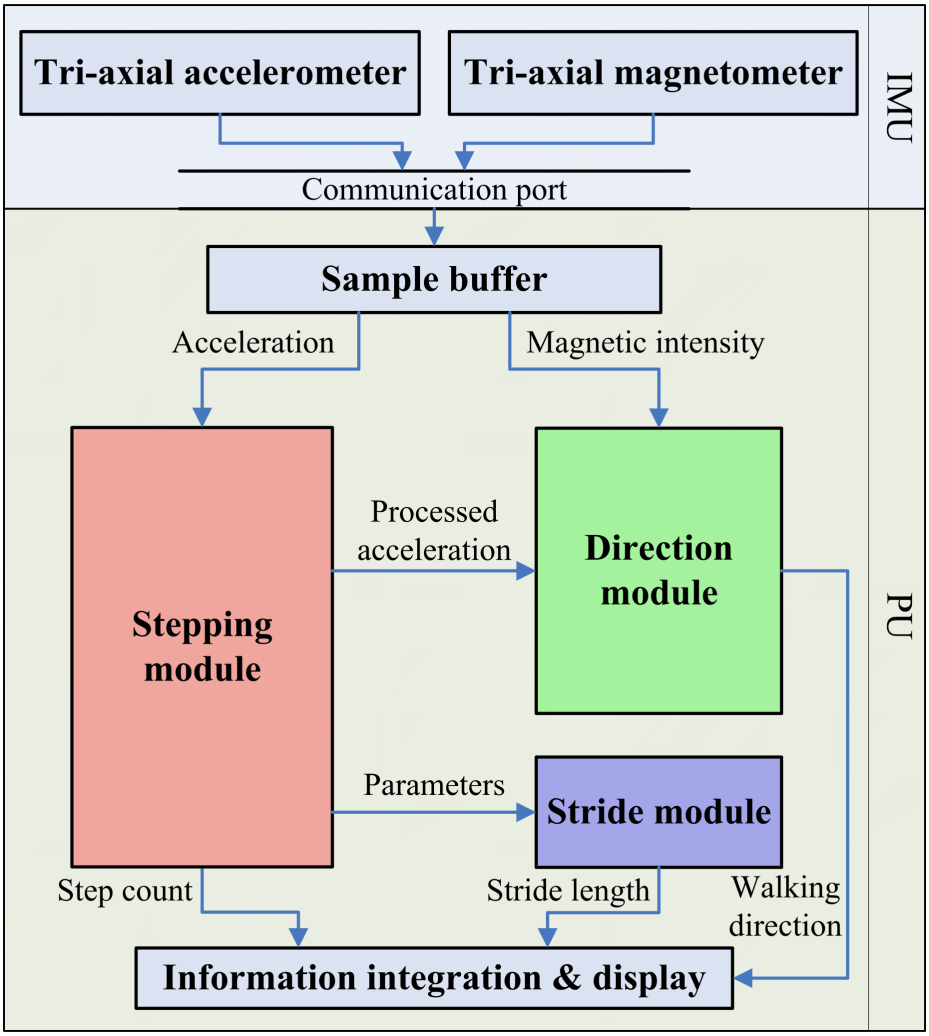

Figure 3.1: System architecture of PTS.

tion module. The stepping module, including the acceleration decomposition module, the step detection module and the noise filter as Figure 3.2, acquires the accelerometer output and determines the step occurrence using acceleration. The stride module acquires the parameters, which are calculated

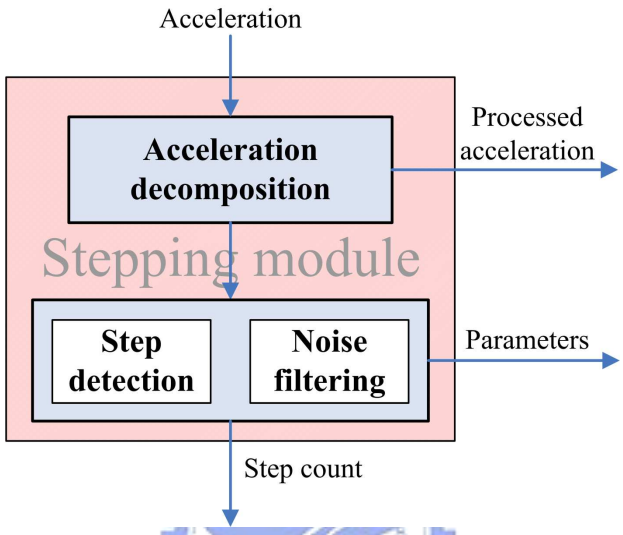

Figure 3.2: Stepping module architecture.

through step module and used for step detection, from the stepping module and uses them to estimate the stride length of a user. The direction module, which is composed of the holding angle module and Euler angle module as Figure 3.3, acquires the process acceleration information from the step module, then calculates the Euler angle and holding angle, outputs the walking direction of a user. The information about the step count, stride length and walking direction is acquired and displayed on the display device.

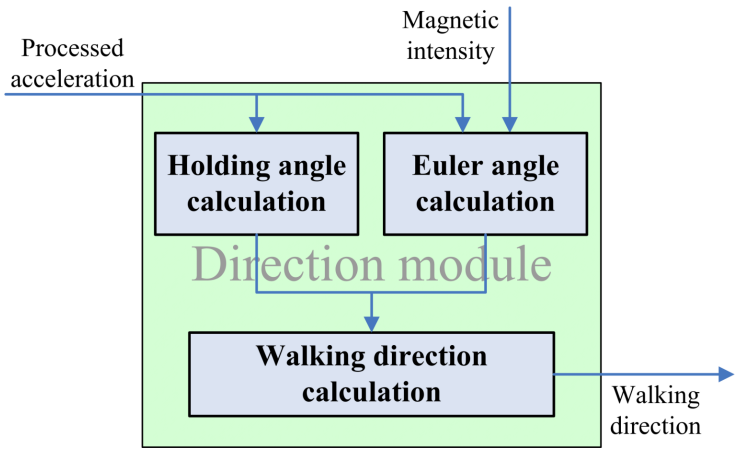

Figure 3.3: Direction module architecture.

Chapter 4

Stepping Module

As described earlier, the accuracy of the step counter is the key to the pedometer-based PNS. To improve the positioning accuracy of the pedometer-based PNS, a robust step detection system is necessary. The goal is very apparent: we cannot overcount or undercount the steps.

In Section 4.1, we introduce how to purify the accelerometer output by decomposing it into two parts: vertical and horizontal accelerations. In Section 4.2 we introduce the step detecting algorithm, and the algorithm is enhanced to detect steps for stair walking in Section 4.3. In Section 4.4, the noise filter is illustrated.

4.1 Acceleration Decomposition

The output of accelerometer is decomposed into two components: z (vertical) and xy (horizontal). The z component is the component of accelerometer reading in the direction of the gravity. Since the wearing orientation of the tri-axial accelerometer is not fixed at the human body, the z direction is in fact unknown. The z direction is obtained by average the accelerometer reading for a period of time as the accelerometer remains static. We adopt this approach by including a simple threshold to filter the hyperactive accelerometer output. Specifically, let $\overrightarrow{A}_{i-m}$, $\overrightarrow{A}_{i-m+1}$,..., $\overrightarrow{A}_{i-1}$ be the accelerometer

output vectors over the period. We first filter out those vectors that are below a lower bound L_g or over an upper bound U_g. Then the average of these remaining vectors, denoted by $\overrightarrow{A}_i^g$, is a vector along the z direction. This approach accommodates the $\overrightarrow{A}_i^g$ to a dynamic environment such as human walking.

According to $\overrightarrow{A}_i^g$, we decompose the next vector $\overrightarrow{A}_i$ into z- and xy-components. As Figure 4.1 shows, the z-component of $\overrightarrow{A}_i$ is calculated as

$$\overrightarrow{A}_i^z = \frac{\overrightarrow{A}_i \cdot \overrightarrow{A}_i^g}{\left|\overrightarrow{A}_i^g\right|^2} \overrightarrow{A}_i^g. \tag{4.1}$$

It follows that the xy-component of $\overrightarrow{A}_i$ is

$$\overrightarrow{A}_i^{xy} = \overrightarrow{A}_i - \overrightarrow{A}_i^z. \tag{4.2}$$

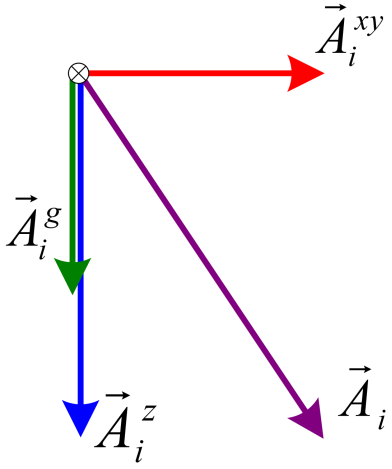

Figure 4.1: Acceleration decomposition.

4.2 Step Detection - Flat Case

A pattern matching method is used for detecting the occurrence of step. The variations of vertical acceleration when a user walks are used to recognize the

walking pattern. The vertical acceleration we use here means $\left|\overrightarrow{A}_i^z\right| - \left|\overrightarrow{A}_i^g\right|$. Because $\left|\overrightarrow{A}_i^z - \overrightarrow{A}_i^g\right|$, the norm of the inertial vertical acceleration, is always positive, we use $\left|\overrightarrow{A}_i^z\right| - \left|\overrightarrow{A}_i^g\right|$ instead to extract more information.

Figure 4.2 shows the vertical acceleration while a subject straight walks 5 steps. There are five cosine-like waveforms. A waveform which includes

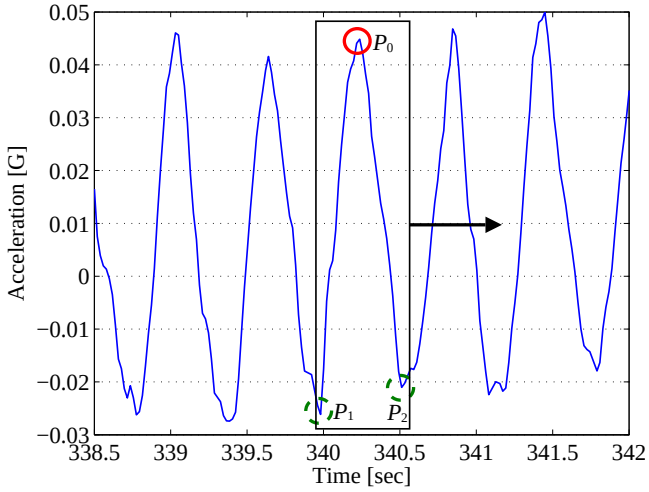

Figure 4.2: Use sliding window technique (solid square) to capture a step pattern in the vertical acceleration while a subject walks 5 steps.

one peak and two troughs is recognized as a step pattern. A step pattern is a candidate for a real step. To detect this pattern, a sliding window (solid square in the figure) is placed on the vertical acceleration samples and used for scanning vertical accelerations in real time. The window size is fixed, and correlates with the sampling rate of device and the duration of step cycle. If the size is too small, the step pattern cannot be appeared. On the contrary, if the size is too large, the window will contain more than one waveform, leading a underestimate for the step count. It is because that there is a risk that wrong step pattern might be recognized, and it will be discussed later. Therefore, the sliding window size should be adjust to contain only one single step pattern for preventing step lost.

The system recognizes a step pattern by the following steps: 1) the system searches the point with the maximum acceleration in the window, and denote this point by P_0 and mark it with a solid circle in Figure 4.2; 2) the window searches backward (left of P_0) for P_1, the left point with minimum acceleration in the window, and forward (right of P_0) for P_2, the right point with minimum acceleration in the window. Both P_1 and P_2 are marked with a dash circle each in Figure 4.2. The step pattern is formed by P_1-P_0-P_2. After checking the step pattern with a noise filter (detail is later), we can make sure if the step pattern represents a real step. The sliding window will start from P_2 to avoid counting duplicately after this pattern is determined as a normal step. Otherwise, the window slides forward by several samples. Thus, it is normal that a point may be checked in different time slot, in other words, the P_2 of step n may be the P_1 of step $n+1$.

4.3 Step Detection - Stair Case

Different walking scenarios, such as walking in a flat plane and walking upstairs, will result in the same kind of cosine-like but different period or amplitude waveforms. Take stair walking as an example, the time period and amplitude of the step pattern in stair walking case are greater than those in flat walking case. The reason is that while a user goes downstairs, the height difference between each stairstep will cause stronger impact and the user also needs to spend more time walking the stairsteps while going upstairs. Hence the duration of a step cycle extended. For these reasons, the height and width of the sliding window are greater than those in flat walking.

Figure 4.3 shows the vertical accelerations in flat walking, same as Figure 4.2, with extended sliding window, and the P_1-P_0-P_2 waveform should be chosen as a step pattern in normal situation. In fact, there are two step patterns in the window, and P_3 is higher than P_0, P_4 is lower than P_2,

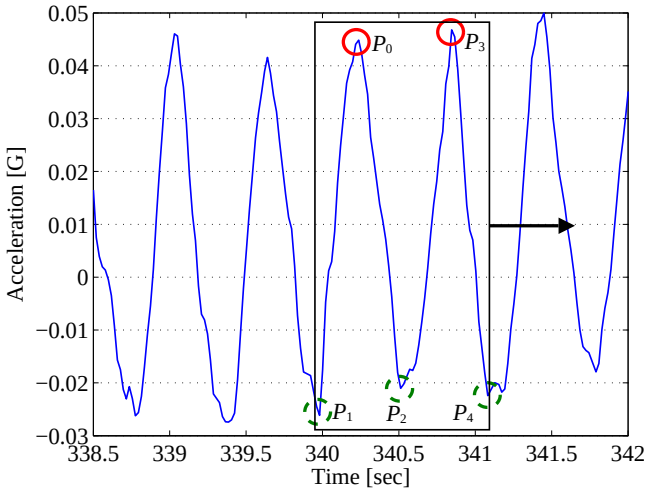

Figure 4.3: Apply an extended sliding window to the vertical accelerations during a subject walks on a flat plane.

resulting in P_3, P_1 and P_4 are chosen. Thus a wrong step pattern candidate is ready to be examined. If the outcome of checking process is true, the window will start from P_4 and lose one step. Or, the window slides forward and checks the same pattern again. It is still false until the P_1 and P_0 are out of window and this also leads to the same result: one step is lost. Finding a window size applicable in all cases is difficult. Thus, the double sliding windows are used instead of single sliding window.

As shown in Figure 4.4, an additional smaller sliding window (dash square in the figure) is fixed into the larger one on the center of it. The sizes of the outer window and inner window are defined as W and w respectively. The system searches the maximum acceleration in the inner window as P_0. To prevent choosing wrong maximum, w is small enough to contain only one peak and satisfies that $w < S$, where S is the shortest duration of a step pattern. After finding P_0, system starts to search for P_1 and P_2 in the outer window, it should contain just two minimums and the size of it satisfies $W < 3S$. Then, the checking process begins to start. Figure 4.4 shows the

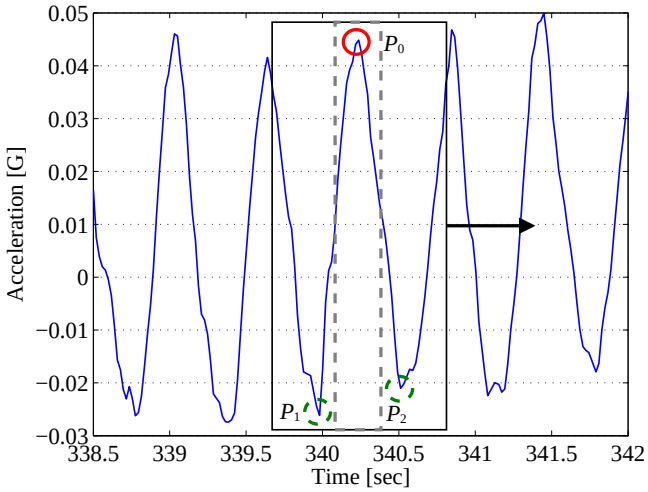

Figure 4.4: Use double sliding windows technique in the vertical accelerations during a subject walks 5 steps on a flat plane.

double sliding windows technique is applied in flat walking case and Figure 4.5 shows the same technique applied in stair climbing case.

4.4 Noise Filtering

To check if a step pattern candidate is a normal step, some parameters or indices are defined. Each parameter has its own lower bound $L_\cdot$ and upper bound $U_\cdot$, and these bounds also can be figured out from experiments. This checking process is called as noise filtering.

In Figure 4.2, let the coordinates of P_i are (t_i, a_i) for $i = 0, 1$ and 2. Define $T = t_2 - t_1$, the duration between P_1 and P_2. People usually walk in a regular frequency, hence the time interval of each step is bounded. The durations induced by shaking or vibrations are beyond the regular range of T, so they are easy to be discarded through the following restriction on a normal step:

$$L_T < T < U_T. \qquad \text{(Cond. 1)}$$

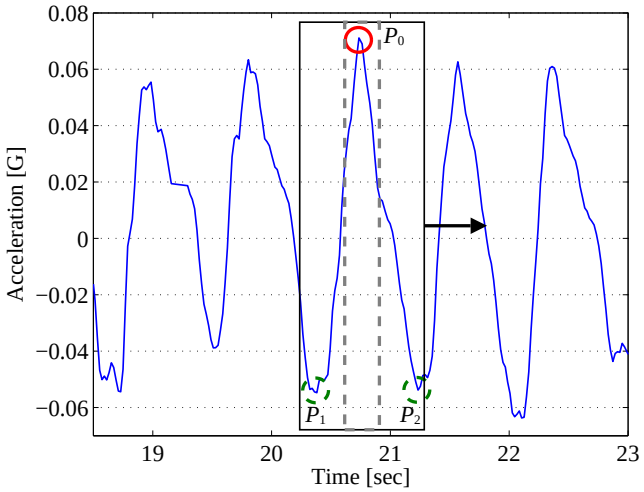

Figure 4.5: Use double sliding window technique in the vertical accelerations during a subject goes downstairs 5 steps.

Define

$$\Delta A_1 = a_0 - a_1 \tag{4.3}$$

and

$$\Delta A_2 = a_0 - a_2. \tag{4.4}$$

Similarly, ΔA_1 and ΔA_2 for shaking or vibrations are also beyond the regular scope for walking, so they are easily weeded out by

$$L_{\Delta A} < \Delta A_i < U_{\Delta A},\ i = 1, 2, \tag{Cond. 2}$$

where $L_{\Delta A}$ and $U_{\Delta A}$ represent the common lower bound and the common upper bound of ΔA_i respectively. Another parameter R_A , the ratio of ΔA_1 to ΔA_2, is near 1 in normal step case. By checking the following condition of R_A,

$$L_{R_A} < R_A < U_{R_A}, \tag{Cond. 3}$$

we can decide whether a pattern is a normal step or not.

Let $\left|\overrightarrow{A}_i^{xy}\right|$ be the norm of the horizontal acceleration of the i-th data counting from P_1 and l the sample number from P_1 to P_2. Define I^h, the

magnitude of horizontal accelerations, as

$$I^h = \sum_{i=0}^{l} \left| \overrightarrow{A}_i^{xy} \right| \Delta t. \tag{4.5}$$

Walking will cause a change in accelerations not only in the vertical axis but also in the horizontal axis. A subject's jumping will cause strong accelerations in vertical axis and less in horizontal axis, thus the horizontal accelerations are sum as the magnitude index of forward accelerations. I^h is examined for helping judge if a user is jumping by

$$L_{I^h} < I^h < U_{I^h}. \tag{Cond. 4}$$

The Fast Fourier Transform (FFT) is also applied to evaluate the measured step pattern. In FFT, finite periodic functions x_n could be written as

$$x_n = \frac{1}{N} \sum_{k=0}^{N-1} X_k e^{i\frac{2\pi}{N}kn}, \; n = 0, \ldots, N-1, \tag{4.6}$$

where X_k indicate the Fourier magnitude at frequency k, n is the sample number in time domain, and N is the amount of the components. The $e^{i\frac{2\pi}{N}kn}$ could be represented as

$$e^{i\frac{2\pi}{N}kn} = \cos\frac{2\pi}{N}kn + i\sin\frac{2\pi}{N}kn, \tag{4.7}$$

which is the sum of sines and cosines. In other words, while the curve of x_n is similar to the composite of m sines or cosines, the value of X_m would be outstanding. The sequence x_n are transformed into X_n by the FFT according to the formula:

$$X_k = \sum_{n=0}^{N-1} x_n e^{-i\frac{2\pi}{N}kn}, \; k = 0, \ldots, N-1. \tag{4.8}$$

Let x_n be the sequence of vertical accelerations from P_1 to P_2 and transform them from time domain to frequency domain X_n. The high value of X_1 may

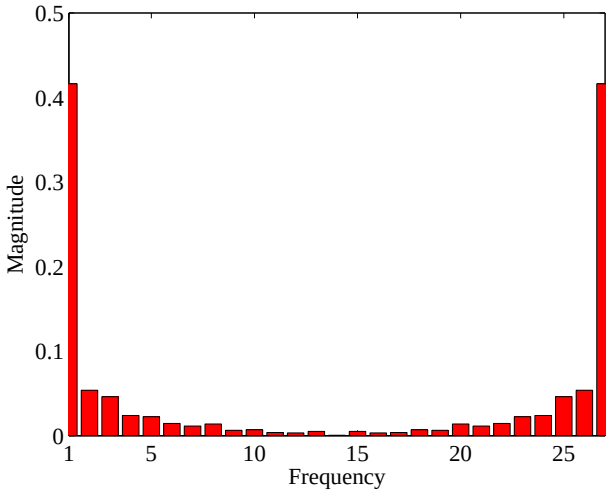

Figure 4.6: The FFT transform results of the samples from P_1 to P_2 in Figure 4.2. The magnitude at frequency 1 which is defined as X_1 is the greatest one.

indicate there is only one cosine-wave in a step pattern. Figure 4.6 shows the transform results of the step pattern within the sliding window in Figure 4.2. Finally, the value of X_1 obtained by FFT of a step pattern is checked through the condition:

$$L_{X_1} < X_1 < U_{X_1}. \qquad \text{(Cond. 5)}$$

By finding the peak and troughs in the sliding window and checking the values of the parameters above, the step occurrence is determined. Figure 4.7 summarizes the flowchart of step detection and noise filtering.

4.5 Experimental Results

Two kinds of experiments are performed to verify the accuracy and reliability of step detection module. The acceleration samples are logged in 50Hz, and Table 4.1 lists the threshold settings for detecting steps and filtering noises.

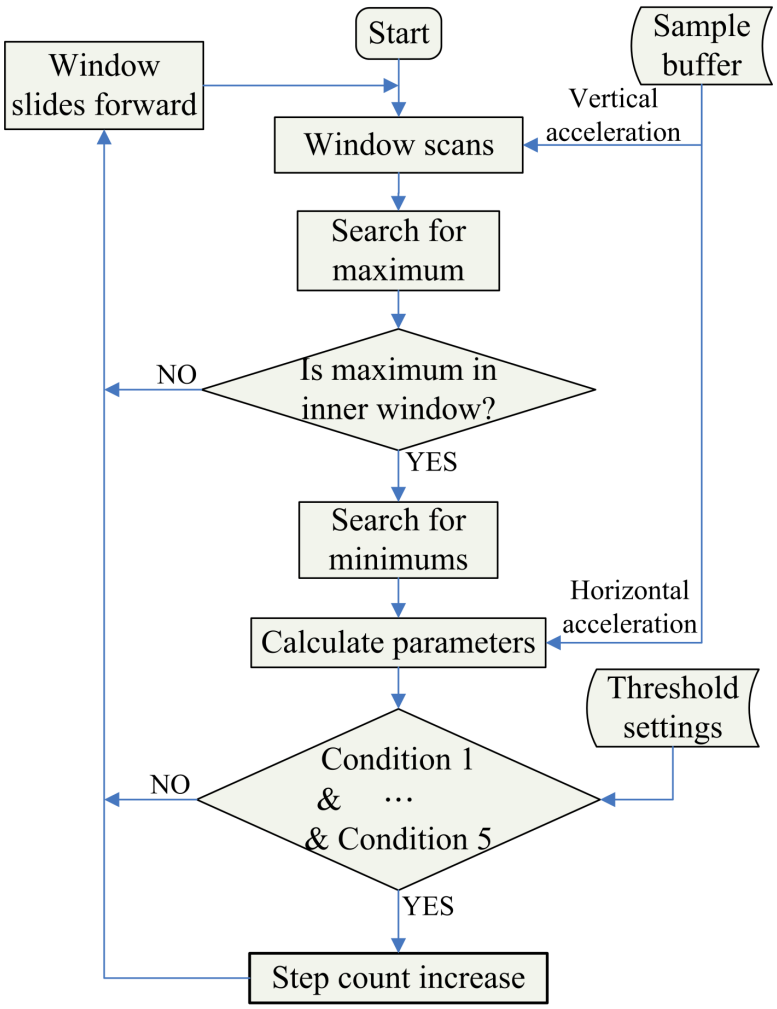

Figure 4.7: Flowchart of step detection and noise filtering.

Table 4.1: Threshold settings for step detection and noise filtering.

Item	Value	
	Lower bound	Upper bound
w	10	
W	42	
$\left\|\overrightarrow{A}^g\right\|$	0.9775	1.02
T	0.3	0.84
ΔA_1 and ΔA_2	0.0095625	0.28
R_A	0.5	3
I^h	0.006	0.142375
X_1	0.057375	1.7

4.5.1 Step Detection Accuracy

In this experiment, each of five subjects held the accelerometer and followed two types of pre-defined courses. One is walking 100 steps on the flat corridor freely with no specified speed, direction and route constraints. The other is going upstairs from the first floor to the third floor, then turning 180° and going downstairs to the first floor. There are 23 stairs between each floor, thus each of the subjects will walk 92 stairs totally. The experimental results of flat walking are illustrated in Table 4.2. The average accuracy is above 95

Table 4.2: Accuracy of step detection in flat walking case.

Subject	Total steps	Step counts	Accuracy
A	100	100	100.00%
B	100	98	98.00%
C	100	95	95.00%
D	100	96	96.00%
E	100	98	98.00%
Average	100	97.4	97.40%

percent in flat walking case and there is a very low rate of step lost in our

system. Table 4.3 and Table 4.4 show the stair walking case experimental results. The accuracy of going downstairs is lower than both going upstairs

Table 4.3: Accuracy of step detection in going upstairs case.

Going upstairs			
Subject	Total steps	Step counts	Accuracy
A	46	45	97.83%
B	46	46	100.00%
C	46	42	91.30%
D	46	45	97.83%
E	46	40	86.96%
Average	46	43.6	94.78%

Table 4.4: Accuracy of step detection in going downstairs case.

Going downstairs			
Subject	Total steps	Counting steps	Accuracy
A	46	41	89.13%
B	46	42	91.30%
C	46	41	89.13%
D	46	37	80.43%
E	46	39	84.78%
Average	46	40	89.86%

and flat walking because the subjects sometimes jumped from one stair to the next one. Jumping causes abnormal accelerations, resulting in the raise of system error rate. If some thresholds are loosed, the noise-proof ability would be reduced. It is a tradeoff between step detection accuracy and noise resistance.

4.5.2 Noise Resistance

In this experiment, each subject shakes and swings the accelerometer with any direction and strength 100 times, and the system records the step counts. Table 4.5 lists the statistics of this experiment. The results exhibit a strong noise resistance by step detection module.

Table 4.5: Performance of noise filter.

Subject	Shaking times	Step counts	Filtered rate
A	100	3	97.00%
B	100	1	99.00%
C	100	2	98.00%
D	100	4	95.00%
E	100	2	98.00%
Average	100	2.4	97.60%

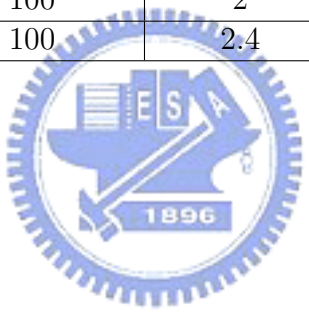

Chapter 5

Stride Module

Because the step detection module described in previous chapter has no capability of calculating the walking distance of user, a stride length estimation module is required. It acquires the parameters of the step pattern from the stepping module and uses them to calculate the stride length. By sum the stride length every step, the total walking distance of user is derived.

In Section 5.1, we introduce why we use regression analysis, and what parameters are used for estimating the stride length. How to evaluate the transform equations between a step pattern and stride length are illustrated in Section 5.2.

5.1 Variable Selection

After careful consideration, the regression analysis method is chose as the method of estimating stride length in the proposed system rather than the double-integration method. Because a foot-mounted accelerometer senses zero velocity and acceleration when the user's foot touches the ground fully. This feature is helpful to eliminate the accumulative errors produced by the integration process. Nevertheless, in handheld posture, the accelerometer always senses a lot of vibrations which caused by user's hand, and it is hard to ask user to freeze his hand for correcting the results of double-integration.

Thus, the regression analysis method is more suitable than double-integration method for handheld posture.

Let D be the stride length of a step pattern, x be the parameter of a step pattern, we use regression analysis to obtain the regression equation d as follow

$$D = d(x) \tag{5.1}$$

where D is the dependent variable, and x is the independent variable used in regression analysis.

First, a training process was performed for observing and analyzing the variation of parameters. A subject walked straight several steps with steady speed, then, the step parameters and the actual step length were recorded every step. By the way, the first and last step patterns are discarded for eliminating unsteady patterns. The experimental statistics are illustrated in Table 5.1, where ΔA_{sum} indicates the sum of ΔA_1 and ΔA_2, the other parameters are introduced and used for detecting step occurrence in previous chapter. In Table 5.1, the ΔA_{sum} and X_1 show higher correlation between stride length and the value of parameter than other parameters thus this study focuses on analyzing these two parameters.

Table 5.1: The statistics of parameters in the training process.

Stride length (cm)	T	ΔA_{sum}	R_A	I^h	X_1
30	0.6587	0.0643	0.9992	0.0183	0.1327
40	0.6567	0.0874	0.9942	0.0194	0.187
50	0.6497	0.1019	1.0029	0.0204	0.2336
60	0.6065	0.1277	1.0132	0.0236	0.3364
70	0.5877	0.1694	1.0274	0.0252	0.4796
80	0.5878	0.2099	1.0643	0.0311	0.6191

5.2 Regression Analysis

A lot of experiments are performed for sample collection. Figure 5.1 shows the experimental statistics and illustrates the relationship between ΔA_{sum} and the stride length. The curve in it is similar to a parabola rather than

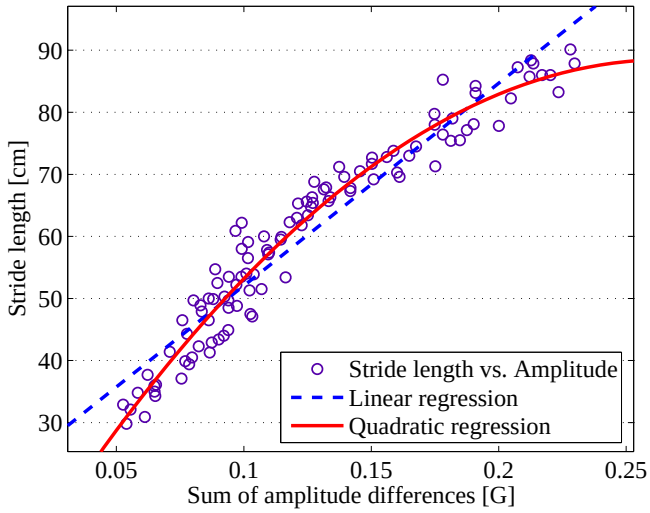

Figure 5.1: The relationship between ΔA_{sum} and stride length with regression equations.

an oblique line. Therefore, not only the linear equation (dash line), but the quadratic polynomial equations (solid line) are also used in the following analyses. The same feature appears in X_1 as Figure 5.2, too. Table 5.2 illustrates the coefficients and r^2 of the regression equations, and the r^2, which measures how successful the equation is in explaining the variation of the stride length, is evaluated through

$$r^2 = 1 - \frac{\sum_i (y_i - d_i)^2}{\sum_i (y_i - \overline{y})^2} \tag{5.2}$$

where y_i is the measured stride length, $\overline{y}$ indicate the average of y_i, and d_i is the estimated stride length. The r^2 indicates a good estimation while it is

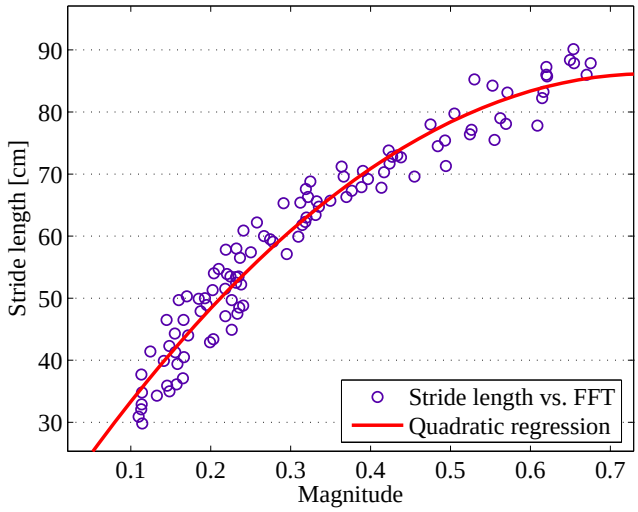

Figure 5.2: The relationship between X_1 and stride length with quadratic regression.

close to 1, and all the values of r^2 in quadratic regression are greater than the corresponding one in linear regression.

Table 5.2: Coefficients and r^2 of the regression equations, where $d(x) = p_1 + p_2 x + p_3 x^2$.

Linear				
x	p_1	p_2	p_3	r^2
ΔA_{sum}	19.427	326.33	0	0.9239
X_1	29.873	93.627	0	0.9135
Quadratic				
x	p_1	p_2	p_3	r^2
ΔA_{sum}	-2.1	681	-1279.6	0.9542
X_1	15.819	187.7747	-125.2949	0.949

Because both r^2 of quadratic equations are similar and close to 1, we consider using multiple regression analysis, which uses multiple independent variables, to improve the estimating accuracy. We set ΔA_{sum} and X_1 as the independent variables, and Table 5.3 illustrates the coefficients and r^2 of the

evaluated multiple linear and quadratic regression equations.

Table 5.3: Coefficients and r^2 of the multiple regression equations, where $d(x, y) = p_1 + p_2x + p_3y + p_4xy + p_5x^2 + p_6y^2$.

	p_1	p_2	p_3	p_4	p_5	p_6	r^2
Linear	21.4971	258.6245	19.7258	0	0	0	0.9247
Quadratic	-4.9	1011.9	-95.7	5097.7	-9706.9	-778.2	0.9591

The values of r^2 both in linear and quadratic multiple regression equations are greater than the corresponding ones in Table 5.2, thus we consider that the multiple regression equation is more reliable than the equations only uses one independent variable. Figure 5.3 shows the result of multiple regression analysis. Let D be the estimated stride length, the estimating equation in

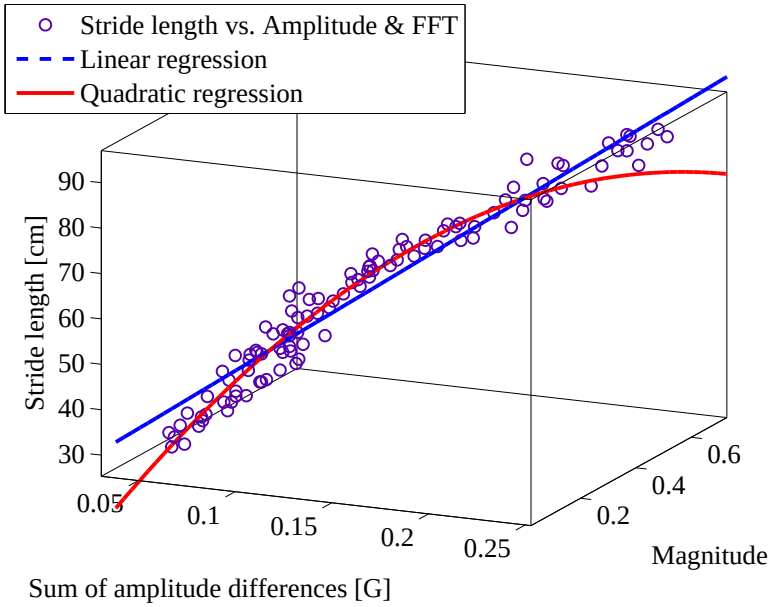

Figure 5.3: Result of multiple regression analysis.

our system is defined as follow:

$$D = -4.9 + 1011.9\Delta A_{sum} - 95.7X_1 + 5097.7\left(\Delta A_{sum}\right)\left(X_1\right) \\ - 9706.9\left(\Delta A_{sum}\right)^2 - 778.2\left(X_1\right)^2. \tag{5.3}$$

Thus, the stride length corresponds to a step pattern is estimated.

5.3 Experimental Results

In this experiment, each of six subjects held the accelerometer and walked straight 20 steps with unrestricted stride length. The total walking distance is measured after, and the estimated distance which is the sum of the estimated length each step is recorded. Table 5.4 shows the experimental results of stride length estimation, and the results of multiple linear regression $d\left(A, X\right)$ and multiple quadratic regression $d^2\left(A, X\right)$ are compared.

Table 5.4: Accuracy of stride length estimation.

Subject	Total distance (m)	$d\left(A, X\right)$	Accuracy	$d^2\left(A, X\right)$	Accuracy
A	13.06	12.29	94.13%	12.77	97.77%
B	11.21	11.93	93.58%	11.61	96.40%
C	12.52	13.28	93.96%	13.40	92.97%
D	11.57	12.08	95.61%	12.24	94.23%
E	11.07	11.00	99.38%	11.23	98.55%
F	10.70	11.27	94.70%	10.98	97.38%
Average			95.23%		96.22%

Chapter 6

Direction Module

The walking distance of a user is computable through integrating the outcomes of the stepping module and stride module, but the exact location is still unknown without a walking direction calculation module. Assume the initial position of the user is known, the trajectory of him is computable by integrating the walking distance and walking direction. The direction module is designed to calculate the walking direction of user for personal positioning, it calculates the orientations of device and the heading direction of human.

In Section 6.1, we give the definitions of the coordinate system and the rotation matrices. In Section 6.2, we describes how to calculate the Euler angles, which indicate the orientations of the device, by using magnetometer and accelerometer information. An issue of the holding angle of a handheld devices which affects the walking direction calculation in a DR module is discussed next. How to calculate the forward acceleration, which is used for evaluating the holding angle, is described in Section 6.3. In Section 6.4, the method of calculating holding angle by quaternion is introduced.

6.1 Rotation Matrices

First, we give the definitions of the body coordinate system, Earth coordinate system and the rotation sequence between them. The body coordinate

system is fixed to the device, including accelerometer and magnetometer, and rotates with it, the x-axis of it points forward when it is placed on a flat plane, the y-axis points to the right of it, and the z-axis points downward. The Earth coordinate system is fixed to the Earth and the x-axis of it is always pointing to north, y-axis pointing to east, and the z-axis pointing to the center of Earth, like the gravity. The Earth coordinate system is transformed to the body coordinate system by the following: 1) rotate around the z-axis by the yaw (ψ) angle; 2) rotate around the new y-axis by the pitch (θ) angle; and 3) rotate around the new x-axis by the roll (φ) angle. All the rotations above are right-handed, and three rotation matrices are established as follows:

$$
\begin{aligned}
R_x(\varphi) &= \begin{bmatrix} 1 & 0 & 0 \\ 0 & \cos\varphi & \sin\varphi \\ 0 & -\sin\varphi & \cos\varphi \end{bmatrix} \\
R_y(\theta) &= \begin{bmatrix} \cos\theta & 0 & -\sin\theta \\ 0 & 1 & 0 \\ \sin\theta & 0 & \cos\theta \end{bmatrix} \\
R_z(\psi) &= \begin{bmatrix} \cos\psi & \sin\psi & 0 \\ -\sin\psi & \cos\psi & 0 \\ 0 & 0 & 1 \end{bmatrix}
\end{aligned}
\tag{6.1}
$$

where $R_x(\varphi)$, $R_y(\theta)$ and $R_z(\psi)$ are the rotation matrices around x-, y-, and z-axis, respectively. Therefore, any vector $\overrightarrow{V}^E$, which is measured in Earth coordinate, could be transformed to the vector $\overrightarrow{V}^B$ in body coordinate by the following:

$$
\begin{aligned}
\overrightarrow{V}^B &= R_x(\varphi) R_y(\theta) R_z(\psi) \overrightarrow{V}^E \qquad (6.2) \\
&= \begin{bmatrix} \cos\psi\cos\theta & \sin\psi\cos\theta & -\sin\theta \\ \cos\psi\sin\theta\sin\varphi - \sin\psi\cos\varphi & \sin\psi\sin\theta\sin\varphi + \cos\psi\cos\varphi & \cos\theta\sin\varphi \\ \cos\psi\sin\theta\cos\varphi + \sin\psi\sin\varphi & \sin\psi\sin\theta\cos\varphi - \cos\psi\sin\varphi & \cos\theta\cos\varphi \end{bmatrix} \overrightarrow{V}^E
\end{aligned}
$$

6.2 Euler Angle Calculation

While the device is placed on a plane, the output vector of accelerometer $\overrightarrow{A}^E = \begin{pmatrix} 0 & 0 & -\left|\overrightarrow{A}^g\right| \end{pmatrix}^T$, and the relationship between the calculated gravity $\overrightarrow{A}^g$ and $\overrightarrow{A}^E$ is described as follow:

$$\begin{aligned} \begin{bmatrix} A_x^g \\ A_y^g \\ A_z^g \end{bmatrix} &= R_x(\varphi) R_y(\theta) R_z(\psi) \begin{bmatrix} 0 \\ 0 \\ -\left|\overrightarrow{A}^g\right| \end{bmatrix} \\ &= \begin{bmatrix} \left|\overrightarrow{A}^g\right| \sin\theta \\ -\left|\overrightarrow{A}^g\right| \cos\theta \sin\varphi \\ -\left|\overrightarrow{A}^g\right| \cos\theta \cos\varphi \end{bmatrix} \end{aligned} \tag{6.3}$$

where A_x^g, A_y^g and A_z^g indicate the x-, y- and z-axis components of $\overrightarrow{A}^g$. Thus the tilt angles, including roll and pitch, could be evaluated by using $\overrightarrow{A}^g$ as:

$$\begin{aligned} \theta &= \arcsin\left(\frac{A_x^g}{\left|\overrightarrow{A}^g\right|}\right), \text{ and} \\ \varphi &= \arcsin\left(\frac{-A_y^g}{\left|\overrightarrow{A}^g\right| \cos\theta}\right) \end{aligned} \tag{6.4}$$

To stabilize the calculating results, we use the components of $\overrightarrow{A}^g$ instead of the components of instantaneous accelerometer output. Figure 6.1 and Figure 6.2 are the illustrations of (6.4).

The heading angle, the main purpose in this study, is calculated by using θ, φ, and the magnetometer information. We revise the equations introduced in [10] as follows. First, define three magnetic vectors which are measured by magnetometer: body vector, level vector, and Earth vector. The body vector $\overrightarrow{M}^B = \begin{pmatrix} M_x^B & M_y^B & M_z^B \end{pmatrix}^T$ is the instantaneous magnetometer output, and the level vector $\overrightarrow{M}^L = \begin{pmatrix} M_x^L & M_y^L & M_z^L \end{pmatrix}^T$ is the magnetometer output while

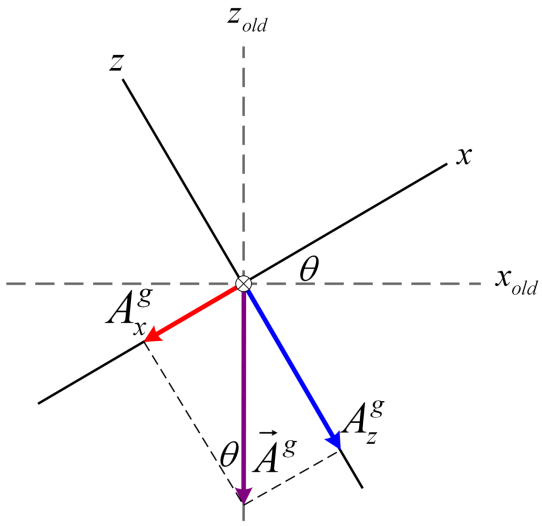

Figure 6.1: Use accelerometer outputs to evaluate pitch angle.

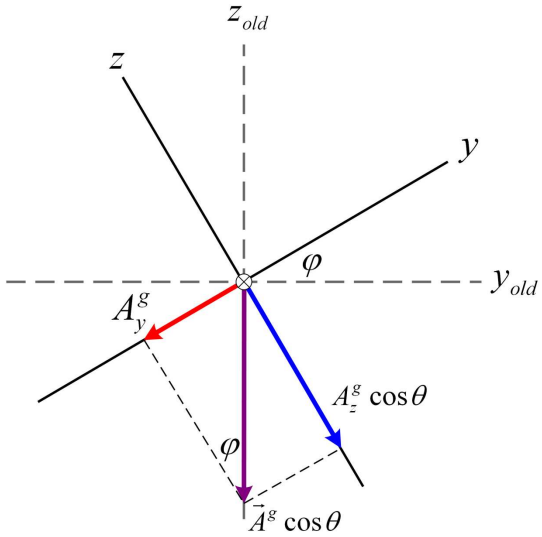

Figure 6.2: Use accelerometer outputs to evaluate roll angle.

the device is placed on a horizontal plane, or both the pitch and roll are zero. The Earth vector $\overrightarrow{M}^E = \begin{pmatrix} M_x^E & M_y^E & M_z^E \end{pmatrix}^T$ is the magnetometer output while the x-axis points to North Pole of the Earth, the y-axis points to East, and the z-axis points to the center of Earth. The components of $\overrightarrow{M}^E$ is based on the inclination and declination of Earth and changes with the longitude and latitude. The relationship between these vectors is described as follows:

$$\overrightarrow{M}^L = R_z(\psi)\,\overrightarrow{M}^E \tag{6.5}$$

$$\begin{aligned}\overrightarrow{M}^B &= R_x(\varphi)\,R_y(\theta)\,\overrightarrow{M}^L \\ &= R_x(\varphi)\,R_y(\theta)\,R_z(\psi)\,\overrightarrow{M}^E\end{aligned} \tag{6.6}$$

To obtain ψ, first we calculate $\overrightarrow{M}^L$ by:

$$\begin{aligned}\begin{bmatrix} M_x^L \\ M_y^L \\ M_z^L \end{bmatrix} &= R_y(\theta)^{-1} R_x(\varphi)^{-1} \overrightarrow{M}^B \\ &= \begin{bmatrix} \cos\theta & \sin\theta\sin\varphi & \sin\theta\cos\varphi \\ 0 & \cos\varphi & -\sin\varphi \\ -\sin\theta & \cos\theta\sin\varphi & \cos\theta\cos\varphi \end{bmatrix} \begin{bmatrix} M_x^B \\ M_y^B \\ M_z^B \end{bmatrix}\end{aligned} \tag{6.7}$$

where $\overrightarrow{M}^B$ is acquired by magnetometer, and the $R_x(\varphi)$ and $R_y(\theta)$ are evaluated through θ and φ, which are obtained by (6.4). The value of M_y^E depends on the declination of Earth, and because the effect of the declination is slight enough to be neglected, we ignore M_y^E and revise (6.5) as:

$$\begin{aligned}\begin{bmatrix} M_x^L \\ M_y^L \\ M_z^L \end{bmatrix} &= \begin{bmatrix} \cos\psi & \sin\psi & 0 \\ -\sin\psi & \cos\psi & 0 \\ 0 & 0 & 1 \end{bmatrix} \begin{bmatrix} M_x^E \\ 0 \\ M_z^E \end{bmatrix} \\ &= \begin{bmatrix} \cos\psi M_x^E \\ -\sin\psi M_x^E \\ M_z^E \end{bmatrix}\end{aligned} \tag{6.8}$$

Thus, the ψ is evaluated by:

$$\psi = \tan^{-1}\left(\frac{-M_y^L}{M_x^L}\right) \tag{6.9}$$

The effect of the inclination is eliminated through this equation, and Figure 6.3 is the illustration of (6.9).

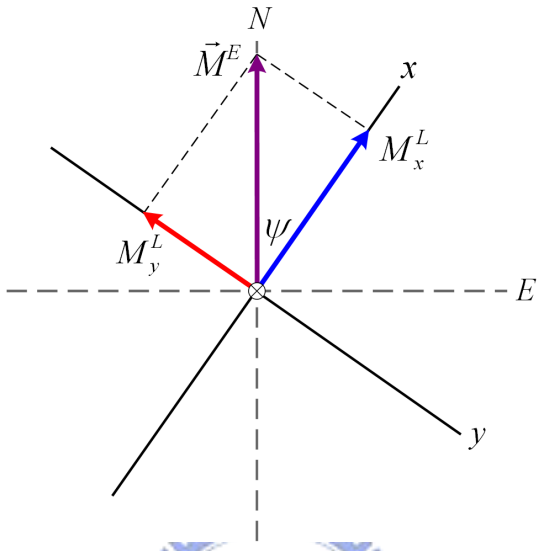

Figure 6.3: Use magnetometer outputs to evaluate yaw angle.

6.3 Forward Acceleration Calculation

Sometimes the user heading direction is different from the handheld device heading direction, it will cause many erroneous computations in direction and location prediction in common DR module because the calculated direction is not the true walking direction. The following sections illustrate an useful algorithm for calculating the pitch, roll and relative yaw angles, which indicate the angle between user heading and handheld device heading, using accelerometer and quaternion. It makes the PTS cope with the situation while the user heading direction is different from the device heading direction.

In theory, walking causes great acceleration in forward and backward directions, and small acceleration in lateral, thus [5] used the principal component analysis to determine the forward direction of a subject with a waist-

mounted device. However, the principal component of horizontal acceleration is not obvious for handheld posture in practice because of the hand vibrations. To figure out the forward acceleration of a human from horizontal acceleration, two conditions are set for filtering the insignificant acceleration vectors: 1) similar to gravity calculation, we set a threshold for horizontal accelerations, but the inactive samples are filtered instead of the hyperactive samples because a great quantity of inactive samples will cover the forward acceleration. Those vectors that are over a lower bound L_F and below an upper bound U_F are filtered out; 2) a feature appearing in the handheld devices is used. It is considered that the forward acceleration of the user usually reflects on the x- and z-axis of a handheld device because user would like to watch the display (the negative of z-axis) of it. Therefore, the z-axis of device is close to the forward acceleration while $\theta \geq 45°$, and the x-axis does so while $\theta < 45°$. This feature helps us judging whether the direction of an acceleration vector is forward or backward, and the forward vectors will not be compensated by the backward vectors. If the z-component of a horizontal acceleration vector is negative, this vector will be filtered out while $\theta \geq 45°$, and a vector whose x-component is negative will be filtered out while $\theta < 45°$, too. After filtering the insignificant vectors through the conditions above, the forward acceleration $\overrightarrow{F_n}$ of user relative to the handheld device is evaluated by accumulating the remaining vectors as:

$$\overrightarrow{F_n} = \sum_{i=n-s+1}^{n} \overrightarrow{A}_i^{xy} \tag{6.10}$$

where s is the required number of sample to evaluate a reliable result. By accumulating the filtered horizontal accelerations, the lateral acceleration would be compensated and only the forward acceleration remains.

The accumulating method makes the forward acceleration of user more stable, but it also results in a problem of cool start, it takes serveral samples

to accumulate $\overrightarrow{F_n}$ in the beginning. To deal with this problem, we propose a method of reversing backward accelerations for reducing the time cost. Because the vectors of forward and bakcward acceleration are in the same axis but opposite directions, thus the reversed backward vectors are similar to the forward vectors. Base on this idea, (6.10) is revised as:

$$\overrightarrow{F_n}' = \sum_{i=n-s+1}^{n} \overrightarrow{A}_i^{xy\prime} \tag{6.11}$$

$$\overrightarrow{A}_i^{xy\prime} = \begin{cases} \overrightarrow{A}_i^{xy}, & \text{if } \theta \geq 45^\circ \text{ and the } z\text{-component of } \overrightarrow{A}_i^{xy} \geq 0 \\ & \text{or } \theta < 45^\circ \text{ and the } x\text{-component of } \overrightarrow{A}_i^{xy} \geq 0 \\ -\overrightarrow{A}_i^{xy}, & \text{otherwise.} \end{cases}$$

By reversing the backward vectors and accumulate them with the forward vectors, the $\overrightarrow{F_n}'$, which is the augmentative $\overrightarrow{F_n}$, takes less time to converge on a reliable result.

6.4 Holding Angle Calculation

The original forward acceleration unit vector of the device is defined as $\overrightarrow{F_o} = \begin{bmatrix} 1 & 0 & 0 \end{bmatrix}^T$. To evaluate the relative Euler angles between $\overrightarrow{F_o}$ and $\overrightarrow{F_n}'$, the quaternion, described and used for dealing with magnetometer outputs in [8], is applied. The rotation axis $\overrightarrow{v} = \begin{bmatrix} v_x & v_y & v_z \end{bmatrix}^T$ and angle δ of the transformation from $\overrightarrow{F_o}$ to $\overrightarrow{F_n}'$ is determined in following:

$$\overrightarrow{v} = \frac{\overrightarrow{F_o} \times \overrightarrow{F_n}'}{\left| \overrightarrow{F_o} \times \overrightarrow{F_n}' \right|} \tag{6.12}$$

$$\delta = \arccos\left(\frac{\overrightarrow{F_o} \cdot \overrightarrow{F_n}'}{\left| \overrightarrow{F_o} \right| \left| \overrightarrow{F_n}' \right|} \right) \tag{6.13}$$

thus the quaternion is:

$$Q = \begin{pmatrix} \cos\left(\frac{\delta}{2}\right) \\ \sin\left(\frac{\delta}{2}\right) v_x \\ \sin\left(\frac{\delta}{2}\right) v_y \\ \sin\left(\frac{\delta}{2}\right) v_z \end{pmatrix} \tag{6.14}$$

The rotation of a vector can be defined by three Euler angles, and the rotation matrix is:

$$R_o^n = R_x(\varphi')R_y(\theta')R_z(\psi') \tag{6.15}$$

where φ', θ', and ψ' indicate the Euler angles calculated by using the accelerometer information, $R_x(\varphi')$, $R_y(\theta')$ and $R_z(\psi')$ indicate the rotation matrix around x-, y- and z-axis, R_o^n is the rotation matrix from $\overrightarrow{F_o}$ to $\overrightarrow{F_n}$. The rotation matrix of quaternion which is equivalent to M_o^n is defined as follows:

$$R_o^{n\prime} = \begin{bmatrix} \cos\delta + (1-\cos\delta)v_x^2 & (1-\cos\delta)v_xv_y - (\sin\delta)v_z & (1-\cos\delta)v_xv_z + (\sin\delta)v_y \\ (1-\cos\delta)v_yv_x + (\sin\delta)v_z & \cos\delta + (1-\cos\delta)v_y^2 & (1-\cos\delta)v_yv_z - (\sin\delta)v_x \\ (1-\cos\delta)v_zv_x - (\sin\delta)v_y & (1-\cos\delta)v_zv_y + (\sin\delta)v_x & \cos\delta + (1-\cos\delta)v_z^2 \end{bmatrix} \tag{6.16}$$

we can evaluate the elements of $R_o^{n\prime}$ by using the elements of Q. Because of the equivalence between $R_o^{n\prime}$ and R_o^n, the yaw, roll and pitch angles are obtained by the following equations:

$$\begin{aligned} \psi' &= \arctan\left(\frac{R_o^{n\prime}(1,2)}{R_o^{n\prime}(1,1)}\right) \\ \theta' &= \arcsin\left(-R_o^{n\prime}(1,3)\right) \\ \varphi' &= \arctan\left(\frac{R_o^{n\prime}(2,3)}{R_o^{n\prime}(3,3)}\right) \end{aligned} \tag{6.17}$$

the ψ' is the orientation difference between user and handheld device. The true walking direction is obtained by summing ψ and ψ'. This information is helpful to eliminate the computation error caused by the heading difference between user and device, and it is an economical solution for tracking relative angles without using gyroscope.

6.5 Experimental Results

There are two experiments: one is for verifying the accuracy of the yaw angle calculation, another is for verifying the accuracy of roll and pitch, and the practicality of holding angle calculation.

6.5.1 Yaw Angle Accuracy

In this experiment, the device, composed of accelerometer, magnetometer and gyroscope, is placed on a horizontal plane and rotates following a predetermined course:

1. Align the x-axis of device to North and y-axis to East by a compass, then start to record the yaw angle.
2. Rotate it clockwise with slow speed for preventing the erroneous computation of gyroscope.
3. Stop for a while when the degree is a multiple of 30° until it reaching 360°.
4. Repeat step 1) - 3) in counterclockwise.

The records of magnetometer are compared with the gyroscope which possesses a high accuracy in short term rotation and synchronized with magnetometer. The full results are illustrated in Table 6.1 and Table 6.2 with the average degree differences between magnetometer and gyroscope. The calculated results of magnetometer exhibits a good accuracy with about 5° errors. However, it is not as good as gyroscope, but it has no accumulative errors and provides the absolute direction information which a gyroscope doesn't provide.

6.5.2 Holding Angle Accuracy

First, we want to decide how many samples should be used for accumulating forward acceleration, thus a training process is performed. The subjects straight walks 60 steps and holds the device with 0° holding angle, the calculating results of $\overrightarrow{F_n}'$, the augmentative $\overrightarrow{F_n}$, are illustrated in the following

Table 6.1: Calculated yaw angles (clockwise), using the magnetometer and gyroscope.

Clockwise				
Degree	Magnetometer	Error	Gyroscope	Error
0°	-0.76°	0.76°	-0.132°	0.132°
30°	28.76°	1.24°	29.796°	0.204°
60°	58.434°	1.566°	60.743°	0.743°
90°	85.406°	4.594°	88.955°	1.045°
120°	114.88°	5.12°	119.832°	0.168°
150°	144.215°	5.785°	149.598°	0.402°
180°	174.573°	5.427°	179.801°	0.199°
210°	203.779°	6.221°	208.132°	1.868°
240°	236.829°	3.171°	239.956°	0.044°
270°	266.897°	3.103°	268.446°	1.554°
300°	296.705°	3.295°	296.96°	3.04°
330°	329.293°	0.707°	328.379°	1.621°
360°	359.083°	0.917°	358.092°	1.908°

Table 6.2: Calculated yaw angles (counterclockwise), using the magnetometer and gyroscope.

Counterclockwise				
Degree	Magnetometer	Error	Gyroscope	Error
0°	-1.564°	1.564°	-0.524°	0.524°
-30°	-31.431°	1.431°	-30.819°	0.819°
-60°	-62.865°	2.865°	-61.543°	1.543°
-90°	-93.068°	3.068°	-90.594°	0.594°
-120°	-122.84°	2.84°	-119.34°	0.66°
-150°	-154.927°	4.927°	-149.867°	0.133°
-180°	-185.57°	5.57°	-179.349°	0.651°
-210°	-215.396°	5.396°	-208.723°	1.277°
-240°	-245.914°	5.914°	-239.062°	0.938°
-270°	-274.717°	4.717°	-268.71°	1.29°
-300°	-301.919°	1.919°	-296.943°	3.057°
-330°	-331.712°	1.712°	-327.738°	2.262°
-360°	-361.779°	1.779°	-358.237°	1.763°

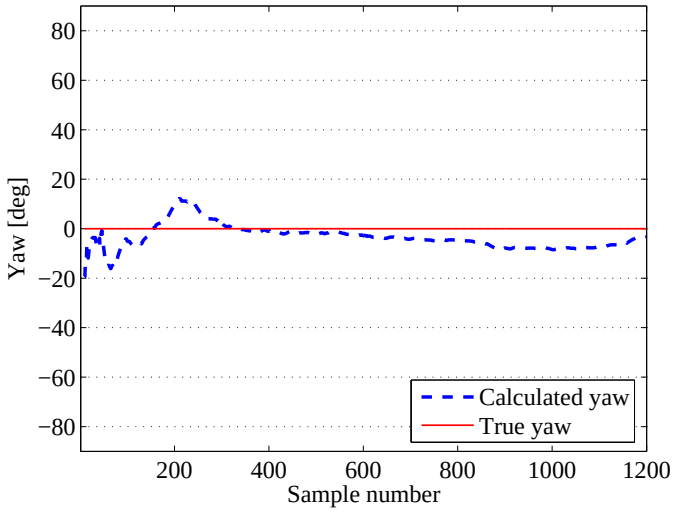

Figure 6.4: A calculating result of yaw using the forward acceleration.

figures. Figure 6.4 shows the calculated yaw angle, Figure 6.5 and Figure 6.6 show the same of pitch and roll, respectively. The long-term pitch and roll, which are considered as the true pitch and roll, are calculated by the long-term $\overrightarrow{A}^g$ (with $m > 1000$) of the corresponding log files in off-line. The results of reversing backward acceleration exhibit a good stability and less degree error than non-reversing backward acceleration in all three Euler angles. It takes about 400 to 600 samples to converge on a reliable result, thus we set s to 600 in the next experiments.

In this experiment, the subjects straight walks 60 steps and holds the device with different holding angles: -40°, -20°, 0°, 20°, 40°. The calculated holding angle ψ' are recorded during the subject walks and compared with the true holding angles in Table 6.3.

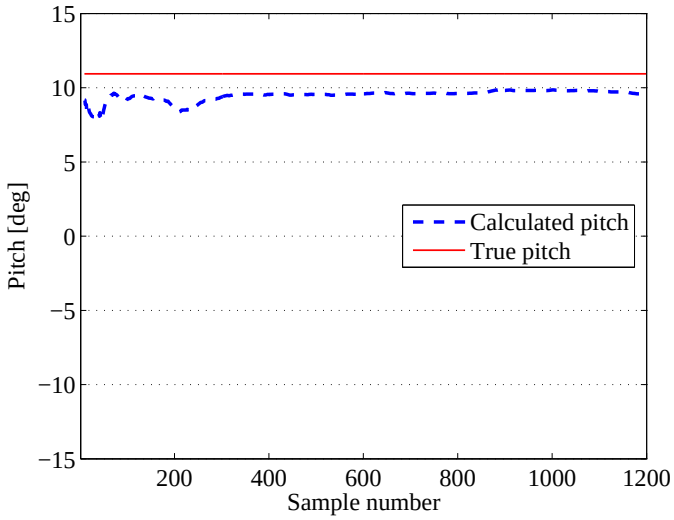

Figure 6.5: A calculating result of pitch using the forward acceleration.

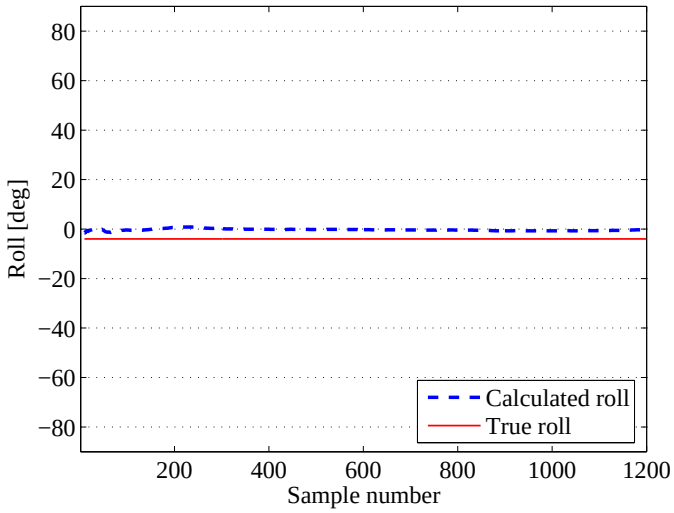

Figure 6.6: A calculating result of roll using the forward acceleration.

Table 6.3: Accuracy of holding angle calculation.

Holding Angle	-40°	-20°	0°	20°	40°
ψ'	-36.765°	-14.95°	-4.682°	17.128°	33.727°
Error	3.235°	5.05°	4.682°	2.872°	6.273°

Chapter 7

Pedestrian Tracking System

By integrating the outputs of stepping module, stride module and direction module, the pedestrain tracking system is implemented. Let D_i be the stride length of i-th step, ϕ_i be the walking direction, which is obtained by integrating the yaw angle and the holding angle of a device, of i-th step. Define $P_i = (x_i, y_i)$ as the displacement of a human after walking i steps, it is represented by the 2-D Cartesian coordinate system and could be simply evaluated by

$$x_{i+1} = x_i + D_i \sin \phi_i \tag{7.1}$$
$$y_{i+1} = y_i + D_i \cos \phi_i$$

where x- and y-axis in our coordinate system points to East and North, respectively.

We performed the experiments with several different routes, the initial position P_0 in these experments is set as (0, 0). The calculated trajectories are recorded and illustrated in the following. Figure 7.1 shows the tracking result of a human walking along a rectangular grassplot in clockwise, and Figure 7.2 is the result of a human walking along an indoor corridor.

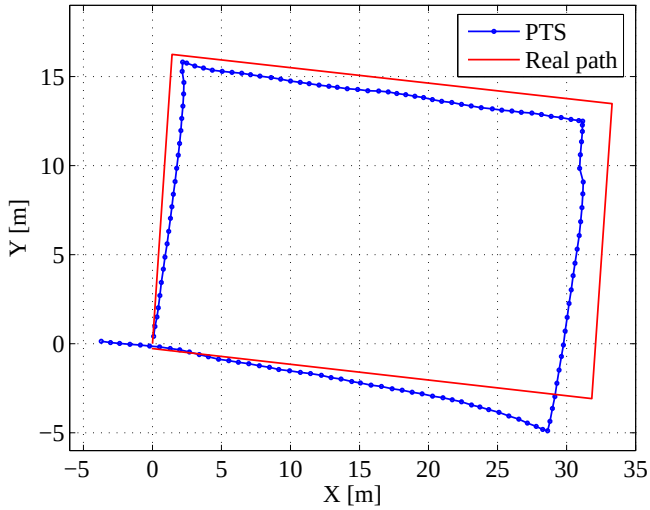

Figure 7.1: Comparison of tracking result and real path in outdoor environment.

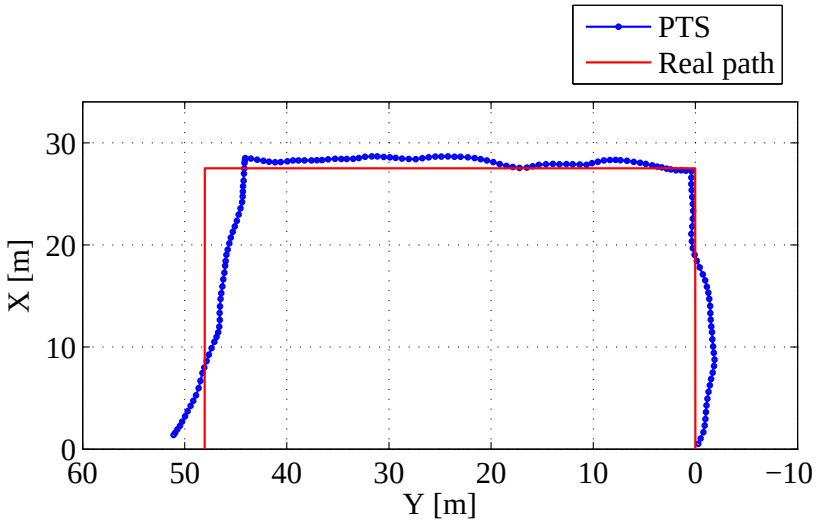

Figure 7.2: Comparison of tracking result and real path in indoor environment.

Chapter 8

Conclusions

In this paper, a pedestrian tracking system is designed for handheld devices and implemented using accelerometers and magnetometers. It is composed of three modules: stepping module, stride module and direction module.

This paper presents some methods to detect pedestrian step occurrence and prevent erroneous step determination for handheld devices. An accurate step detection module is implemented using the accelerometer. The experimental results exhibit an excellent step counting accuracy in flat walking and stair walking case, and possess a stout noise resistance ability.

An useful method of estimating the human walking distance by using the regression analysis is also described. Two specific parameters, including the amplitude and the Fourier magnitude of a step pattern, are used for calculating the stride length. The stride module is implemented using only the accelerometer and integrated with the stepping module to evaluate how long people walks in real time. The accuracy of it is verified by the experiments, it shows a good stride length estimation. The accuracy could be increased by executing more experiments and collecting more parameter samples. The regression analysis is useful for estimating walking distance, but performing the pre-trained process is necessary. It will cost a lot of time for improving the estimating accuracy.

A method of calculating human walking direction is presented, it is able to evaluate a 3-D rotation, which is represented in Euler angles. A holding angle calculating algorithm is proposed next, it is capable of solving the erroneous positioning results, caused by the orientation difference between user and device, of the common DR system.

The PTS is implemented by integrating the outputs of stepping module, stride module and direction module. This system, which can be embedded into cellphones or PDAs easily, is feasible for indoor or outdoor personal positioning with a given initial position. In the future, the PTS could be integrated with the GPS for improving the positioning accuracy of both. It is very helpful for personal navigation in urban areas, indoor and outdoor environments.

In addition, the device sampling rate reduction is also considered for saving energy consumption as a future work. It is possible that all the predetermined thresholds of the parameters for step detection need to be adjusted to recognize the human step pattern effectively in lower sampling rate. However, decreasing the sampling rate of the device may cause a problem that no obvious peaks and troughs appear in acceleration thus step pattern is unrecognizable.

Bibliography

[1] F. Cavallo, A. M. Sabatini, and V. G. Sabatini, "A step toward GPS/INS personal navigation systems: real-time assessment of gait by foot inertial sensing," in *Proceedings of the 2005 IEEE/RSJ International Conference on Intelligent Robots and Systems (IROS 2005)*, 2-6 August 2005, pp. 1187–1191.

[2] X. Yun, E. R. Bachmann, H. Moore, and J. Calusdian, "Self-contained position tracking of human movement using small inertial/magnetic sensor modules," in *Proceedings of the 2007 IEEE International Conference on Robotics and Automation*, 10-14 April 2007, pp. 2526–2533.

[3] J.-A. Lee, S.-H. Cho, J.-W. Lee, K.-H. Lee, and H.-K. Yang, "Wearable accelerometer system for measuring the temporal parameters of gait," in *Proceedings of the 2007 29th Annual International Conference of the IEEE Engineering in Medicine and Biology Society (EMBS 2007)*, 22-26 August 2007, pp. 483–486.

[4] S. H. Shin, C. G. Park, J. W. Kim, H. S. Hong, and J. M. Lee, "Adaptive step length estimation algorithm using low-cost MEMS inertial sensors," in *Proceedings of the 2007 IEEE Sensors Applications Symposium (SAS 2007)*, 6-8 February 2007, pp. 1–5.

[5] M. Kourogi and T. Kurata, "Personal positioning based on walking locomotion analysis with self-contained sensors and a wearable camera," in *Proceedings of the 2003 Second IEEE and ACM International Symposium on Mixed and Augmented Reality*, 7-10 October 2003, pp. 103–112.

[6] A. Y. Jeon, J. H. Kim, I. C. Kim, J. H. Jung, S. Y. Ye, J. H. Ro, S. H. Yoon, J. M. Son, B. C. Kim, B. J. Shin, and G. R. Jeon, "Implementation of the personal emergency response system using a 3-axial accelerometer," in *Proceedings of the 2007 6th International Special Topic Conference on Information Technology Applications in Biomedicine (ITAB 2007)*, 8-11 November 2007, pp. 223–226.

[7] S. Ramat, D. Pré, and G. Magenes, "An internal model of self-motion based on inertial signals," in *Proceedings of the 2006 28th Annual International*

Conference of the IEEE Engineering in Medicine and Biology Society (EMBS 2006), 30 August-3 September 2006, pp. 4961–4964.

[8] A. Fleury, N. Noury, and N. Vuillerme, "A fast algorithm to track changes of direction of a person using magnetometers," in *Proceedings of the 2007 29th Annual International Conference of the IEEE Engineering in Medicine and Biology Society (EMBS 2007)*, 22-26 August 2007, pp. 2311–2314.

[9] Y. Chai, W. Feng, C. Jiang, and K. Liu, "Design and realization of digital compass with magnetometers," in *Proceedings of the 2008 7th World Congress on Intelligent Control and Automation (WCICA 2008)*, 25-27 June 2008, pp. 7672–7675.

[10] K.-H. Lee, J.-W. Lee, K.-S. Kim, D.-J. Kim, K. Kim, H.-K. Yang, K. Jeong, and B. Lee, "Tooth brushing pattern classification using three-axis accelerometer and magnetic sensor for smart toothbrush," in *Proceedings of the 2007 29th Annual International Conference of the IEEE Engineering in Medicine and Biology Society (EMBS 2007)*, 22-26 August 2007, pp. 4211–4214.